The 8th International Supercritical CO_2 Power Cycles Symposium
February 27-29, 2024, San Antonio, Texas
Paper #51

Correlational Model for Heat Transfer Coefficient of Solid Particle-to-CO2 Moving Bed Heat Exchangers with Finned Tubes

Luke R. Magyar
Systems Engineer
Echogen Power Systems
Akron, OH

Dr. Timothy J. Held
Chief Technology Officer
Echogen Power Systems
Akron, OH

Luke R. Magyar is responsible for experimental design and operation of test programs at Echogen Power Systems with a focus on process controls and system modeling. He received a BSChE from the University of Akron in 2018.

Dr. Timothy Held is responsible for development and transition to product of supercritical CO_2 power cycles and energy storage systems. A former gas turbine combustor design engineer and manager at GE Aviation, he received a BSAAE from Purdue University in 1987, and a Ph.D. in Mechanical and Aerospace Engineering from Princeton University in 1993. He has published several technical journal articles and book chapters, and holds 49 U.S. patents.

Abstract

Solid particle-to-CO_2 heat exchangers for use in supercritical CO_2 power cycles are desired for use in both Concentrated Solar Power (CSP) and Pumped Thermal Energy Storage (PTES) applications. Such heat exchangers for use in these cycles are categorized in two major classes—fluidized bed heat exchangers (FBHE) in which heat is transferred indirectly to an embedded tube bundle with circulating air to fluidize the particle bed and moving bed heat exchangers (MBHE) that utilize a low-velocity gravity-driven flow of particles through a stationary heat exchanger. The MBHE has the advantage of simplicity and reduced auxiliary load losses due to the lack of fluidizing air systems. Conventional MBHE construction utilizes a diffusion-bonded "Printed Circuit Heat Exchanger" (PCHE) approach that necessitates the use of nickel-based alloys such as INCONEL® alloys 617, 625, and 740H or Haynes 282 to accommodate the high temperatures and pressures of the CO_2 stream. Tubular MBHE designs allow for thinner wall construction, but without extended fin surfaces, high material costs are still needed to achieve the required heat exchanger surface area. Echogen Power Systems has considered an alternative moving bed heat exchanger design constructed of finned tubes utilizing 316L stainless steel as a fin material, greatly reducing the material costs needed to achieve the target heat transfer area in the heat exchanger. Echogen Power Systems has built a test apparatus to measure the external heat transfer coefficient of finned tubes to solid particles across a battery of geometric parameters and particle flow characteristics. Using the data obtained in this test program, a correlational model for external heat transfer coefficient has been developed to demonstrate the viability of finned tube MBHE technology over more conventional designs.

Introduction

Heat exchange between solid particles and supercritical carbon dioxide (sCO_2) is an important component to power cycle design, in particular for Concentrating Solar Power (CSP) and Pumped Thermal Energy Storage (PTES). In both systems, solid particles, typically quartz sand or sintered bauxite, act as a thermal energy reservoir. For CSP applications, the solid particles are directly heated by solar energy and then flowed through the particle-to-CO_2 heat exchanger to generate electricity with the sCO_2 power cycle. The PTES approach requires the particle-to-CO_2 heat exchanger to operate in both the charge cycle, where energy is transferred to the solid particles, and the generate cycle, where energy is transferred to the CO_2. The two major classes of particle-to-CO_2 heat exchangers are fluidized bed heat exchangers (FBHE) and moving bed heat exchangers (MBHE).

FBHE utilize fluidizing air to convey solid particles through the CO_2 tube bundle, which has the advantage of increasing the convective heat transfer coefficient (HTC) and allowing for bidirectional flow in a horizontally oriented heat exchanger [1]. The major downside of FBHE designs are high parasitic loads, increased costs and complexity, and heat losses caused by the fluidizing air system.

Conventional MBHE designs have been developed for lower fluid pressure applications using a "pillow plate" construction, but these are not suitable for the high pressure required by PTES applications [2]. To address its mechanical shortcomings, the pillow plate can be replaced by diffusion-bonded plates, also known as "Printed Circuit Heat Exchanger" (PCHE) technology [4][5]. To manufacture a PCHE, fluid passages are chemically etched into thin, flat metal plates, which are then stacked together into subassemblies and diffusion bonded in a vacuum furnace under mechanical pressure [12][13]. The resulting bond has mechanical strength comparable to the parent material, enabling construction of complex, large-scale structures. PCHEs have been used successfully, including by Echogen, in sCO_2 power cycles as both recuperators and water-cooled fluid coolers (WCC). In recuperators, heat is transferred from "low"-pressure (7 MPa to 10 MPa) CO_2 to high-pressure (25 MPa to 30 MPa) CO_2 in a counterflow arrangement, while in

WCCs heat is transferred from low-pressure CO_2 to water. PCHEs are compact, and capable of higher pressures than most heat exchanger configurations, other than tubular style heat exchangers.

To obtain good heat transfer performance, a Moving Bed PCHE (MB/PCHE) requires narrow particle passages, and a large number of CO_2 plates. The high temperatures and pressures of sCO_2 power cycles limit the materials of construction to nickel-based alloys, such as INCONEL® alloys 617, 625, and 740H, and Haynes 282. Of these materials, only alloy 617 is presently qualified for use in diffusion-bonded heat exchangers. Material selection represents a significant limitation of the MB/PCHE, wherein the entire heat transfer surface is comprised of a single high-cost material. Their narrow particle passages preclude insertion of additional heat transfer area materials or HTC enhancements that would interfere with the gravity-driven particle flow.

In addition to the monolithic panel construction, the high aspect ratio of the particle passages (length divided by gap spacing) could lead to a higher susceptibility to particle flow irregularities. Small variations in gap spacing are to be expected in a practical device, both from manufacturing tolerances and from thermal and mechanical distortion in service. Because each passage is fed from and discharges to a common hopper, flow rate variation from passage to passage will be exacerbated by the combination of these effects, which was clearly demonstrated in a much shorter flowpath test in Reference [5]. Passage-to-passage variation in flow rate creates reduced heat exchanger effectiveness and localized “hot spots” in passages that receive higher particle flow than the mean. Depending on the severity of the flow maldistribution, significant impacts on material integrity could be expected.

An alternative approach to MBHE construction has been proposed by Baumann and Zunft [*7*], in which a multipass tube-in-crossflow geometry is utilized. A small prototype heat exchanger was built and tested, with particle imaging velocimetry and thermal measurements used to evaluate and improve the design. Key results include the observation of a significant stagnation region upstream of the tubes, and an effective convection HTC that is of comparable magnitude to those found for the MB/PCHE geometry (ca. 200 $W/m^2/K$ to 250 $W/m^2/K$).

An important advantage of the tubular design is that higher-strength materials are available for this configuration than for the MB/PCHE design. In particular, INCONEL alloy 740H is approved by the ASME Boiler and Pressure Vessel Code for Section I construction (Power Boilers) by Code Case 2702, and for construction under ASME B31.1 by Code Case 190 [10]. Alloy 740H has much higher allowable stress than alloy 617 at the temperature ranges of interest for PTES applications, which permits relatively thin-walled construction, thus reducing the amount of material required. However, the drawback of a plain tubular heat exchanger is the limited amount of external heat transfer surface area for a given heat exchanger volume. As the external convection coefficient is considerably lower than the internal coefficient, the thermal resistance of the external heat transfer process becomes the limiting factor in determining the overall heat transfer rate of the system.

The present study considers the addition of relatively low-cost 316L stainless steel fins to tubes constructed of 740H, referred to as the “Moving Bed Finned-Tube Heat Exchanger” (MB/FTHE). Finned-tube designs are an attractive option if the convective HTC is comparable to or in excess of the values measured by Baumann and Zunft for a bare-tube MBHE. Internal cost models at Echogen have suggested MB/FTHE have a significantly lower material and construction cost than MB/PCHE designs, due to the bulk of the heat transfer material volume being comprised of 316L stainless steel. In addition to the material cost advantage, MB/FTHE designs have the potential to achieve higher HTCs than parallel plate designs as the particle flow has the opportunity to mix and “re-start” its thermal boundary layer at every tube row. Finally, the finned tube design is less likely to suffer from the hot spots and flow interruptions to which the parallel plate design is inherently susceptible.

Test System Design

Echogen designed and fabricated a Moving Bed Heat Transfer test facility (Figure 1) to measure the convective HTC of finned tubes in crossflow with solid particles. To facilitate the testing of multiple tube configurations, a test apparatus was designed to allow quick change over of heat exchanger test sections. The system is designed to hold up to 1.0 metric tons of particles in an upper hopper. The test section consists of a square cross-section tube bank through which the particles flow by gravity. The exit cone meters the sand flow through a variable-area slot, which can be adjusted to achieve a target particle mass flow rate as measured by a set of load cells supporting the upper hopper. The converging sections of the exit cone were designed to discourage funnel flow and encourage mass flow of the particles, ensuring a consistent discharge rate with a uniform velocity field across the tube bank [11]. The tube bank was designed with clear polycarbonate walls to provide a visual indication of flow properties, and to facilitate rapid changeover between tube sheet patterns. The use of polycarbonate allowed in-house fabrication of tube sheets that could be swapped without disassembling the structural elements of the test section. The tubes were manufactured from carbon steel, utilizing spiral type fins brazed to the tube surface. The chosen geometric parameters are commonly available sizes relevant to MBHE design for PTES purposes.

To evaluate the convective HTC, a single tube near the center of the heat exchanger test section was equipped with an electric cartridge heater, and several embedded thermocouples within the gap between the heater and the tube internal diameter. To ensure good thermal contact between the heater, thermocouples, and the tube, the gap was filled with molten solder that solidified at the operating temperature. The two transversely adjacent tubes were also electrically heated to reduce the impact of thermal conduction within the particle bed at the measurement

Figure 1: Echogen Moving Bed Heat Transfer test facility. In progress bare tube test shown at right.

location. A variable autotransformer and power monitor were used to adjust and measure the power applied to the heater. After preheating the test element, the flow of particles was initiated and the test proceeded until a steady state was observed in the measured temperatures of the test element.

The particle HTC was calculated by

$$h_{part} = \frac{Q}{A_h \Delta T} \tag{1}$$

where Q is the measured electrical power delivered to the heater, A_h is the heat transfer area, and ΔT is the difference between the test article surface temperature and the free particle bulk temperature. The surface temperature was measured indirectly by the thermocouples embedded in the solder between the tube and cartridge heater, requiring correction for the thermal resistance of the assembly between the heater surface and the tube surface. Direct measurement of the tube surface temperature was not ideal because external thermocouple placement on finned tubes would require grooves to be cut in the fins which would disrupt the particle flow behavior. Low profile adhesive surface mount thermocouples were used in preliminary testing to characterize the thermal resistance of the assembly, but they were not robust enough to withstand repeated testing. Test assemblies of both bare and finned tubes with surface mount thermocouples were evaluated in both water bath and sand crossflow to measure the temperature difference between the heater surface and the tube surface. The thermal resistance correction factor derived from initial testing scaled with power applied to the heater and was consistent between bare-tubes and finned-tubes. The reported h_{part} values were corrected for this thermal resistance.

$$h_{part} = \frac{1}{A}\left(\frac{\Delta T}{Q} - R_{cond}\right) \tag{2}$$

Only the central 20 cm of the 30 cm long tube was heated. To evaluate the impact of the unheated length of tubing on the reported HTCs, a one-dimensional model of the tube was constructed. The tube model included transverse conduction, radial convection and internal bulk heat addition to simulate the impact on calculated HTC versus the “true value” (Figure 2). The model indicated that for HTC values above 100 W/m^2/K, the impact of transverse conduction on the evaluated HTC was less than 10%. Temperature measurements off the centerline of the heated tube were consistent with the thermal model as well. A typical set of temperature measurements during a bare-tube test with quartz sand particles is shown in Figure 3.

A summary of the tested configurations is shown in the Table below. Reported velocities are the maximum velocity calculated from the mass flowrate at the minimum flow area within the tube bundle, accounting for tube spacing, diameter, fin pitch, etc.

ID	Config	Tube		Fin			Particle	Velocity (mm/s)
		Diameter (mm)	Lateral pitch (mm)	Height (mm)	Pitch (1/m)	Thickness (mm)		
B1.1	Bare	19.1	38.1	-	-	-	Sand	4-12
F1.1	Finned	19.1	42.9	9.5	158	0.4	Sand	2-12
F1.2	Finned	19.1	50.8	9.5	158	0.4	Sand	3-11
F1.3	Finned	19.1	50.8	9.5	158	0.4	Bauxite	3-10
B1.2	Bare	19.1	50.8	-	-	-	Bauxite	3-11
F2.1	Finned	19.1	50.8	9.5	276	0.4	Bauxite	2-9
F2.2	Finned	19.1	42.9	9.5	276	0.4	Bauxite	1-6
F3.1	Finned	19.1	42.9	6.4	158	0.4	Bauxite	2-7
F3.2	Finned	19.1	50.8	6.4	158	0.4	Bauxite	2-9
F4.1	Finned	19.1	50.8	9.4	394	0.4	Bauxite	2-10
F5.1	Finned	19.1	50.8	12.7	158	0.8	Bauxite	3-12
F6.1	Finned	25.4	50.8	9.5	158	0.4	Bauxite	2-12

Table 1: Test configurations.

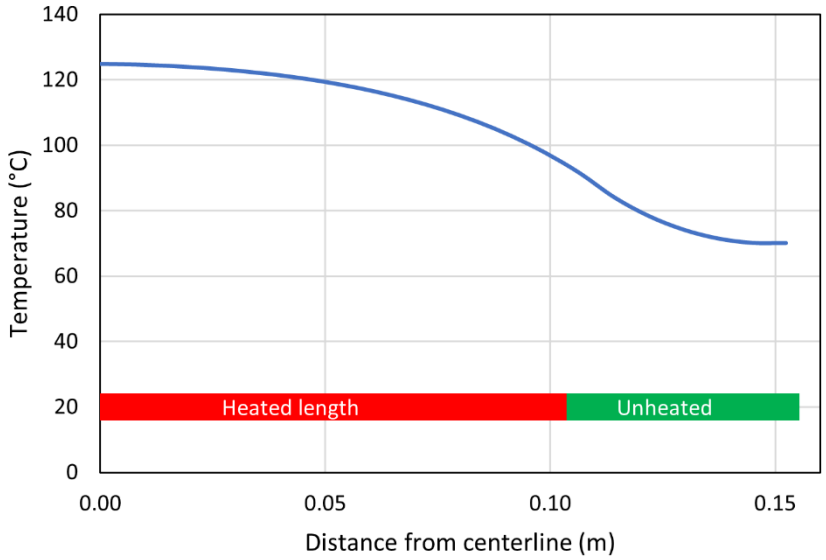

Figure 2: Predicted temperature profile for a representative test condition. The effect of heat losses to the unheated section of the tube on the calculated heat transfer coefficient based on the measured centerline temperature is less than 10%.

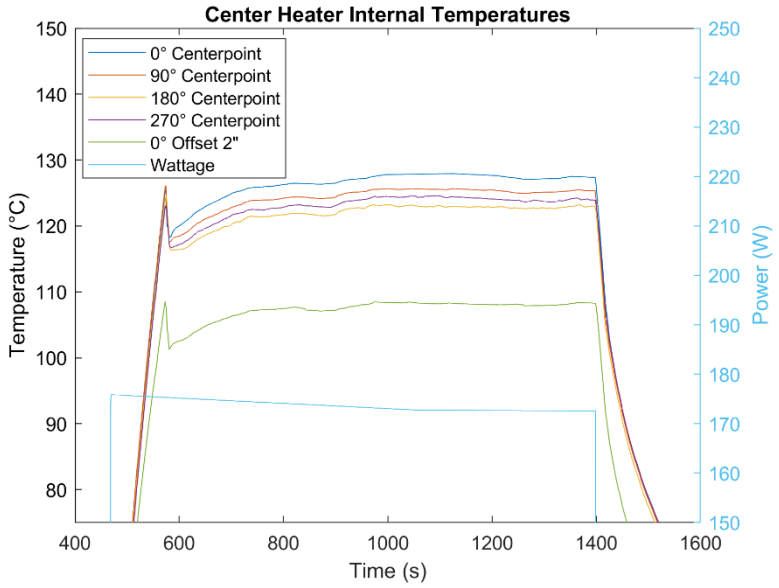

Figure 3: Typical measurements as a function of time during a heat transfer test. The four “Centerpoint” temperature measurements are at the tube centerline, at four circumferential stations relative to the flow direction, while the “Offset” measurement is at the leading edge of the tube, but midway between the centerline and edge of the heated section.

Results

A battery of test conditions was evaluated on the test system to develop correlations for the convective HTC based on tube pitch, tube diameter, fin height, and fin pitch. Additionally, testing was performed using both sand and sintered bauxite to evaluate the effect of material properties on HTC. A baseline test, using bare tubes, was designed to reproduce data from Baumann and Zunft [7]. As can be seen in Figure 4, there is very good agreement between both data sets, validating the experimental approach and data reduction methodology. Error bars from the Baumann and Zunft data are taken from their study, all error bars for data collected in the present work were calculated from the relative instrument error stated by the device manufacturer. Among instruments, amperage meters yield the largest source of relative error at 5% of the measured value, while temperature and voltage measurements were comparatively low at 2%. In addition to the error introduced by measurement, the correction factor $\mathrm{R_{cond}}$ is estimated to have a relative error of 5% based on regression data. Error scales linearly with calculated convective HTC.

Following bare tube baseline testing, finned tubes were installed in the test system and tested over a range of mass flux rates; Figure 5 shows the increase in HTC for a finned tube configuration compared to bare tubes. Note that for this comparison, the HTC is calculated based on the bare tube area which allows for direct comparison of two tubes with differing heat transfer areas. In this case, the true HTC for the finned tubes is 40% less than that of the bare tubes, however, the heat transfer area for the finned tubes is 460% greater than that of the bare tubes.

Figure 6 shows that taken on a basis of mass flux, quartz sand yields a slight increase in HTC compared to sintered bauxite. In Figure 7 the same comparison is made using particle velocity to take the differing particle densities into account. The quartz sand has a mean particle diameter of 170 μm and the sintered bauxite has a diameter of 350 μm. This analysis suggests there is no thermodynamic benefit between quartz sand or sintered bauxite, allowing particle selection for

thermal storage to be decided on other properties that may be favorable for certain applications. The majority of the test data for this study was collected using sintered bauxite because of favorable material handing properties. Unless otherwise noted, all comparisons are made between data sets collected with the same solid media.

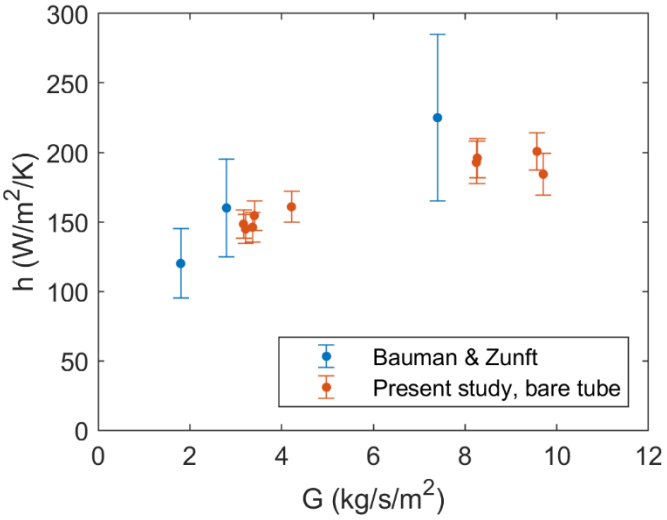

Figure 4: Measured convective HTC vs mass flux for a bare-tube test with quartz sand, compared to geometrically comparable test data from Reference [7]. Test ID: B1.1

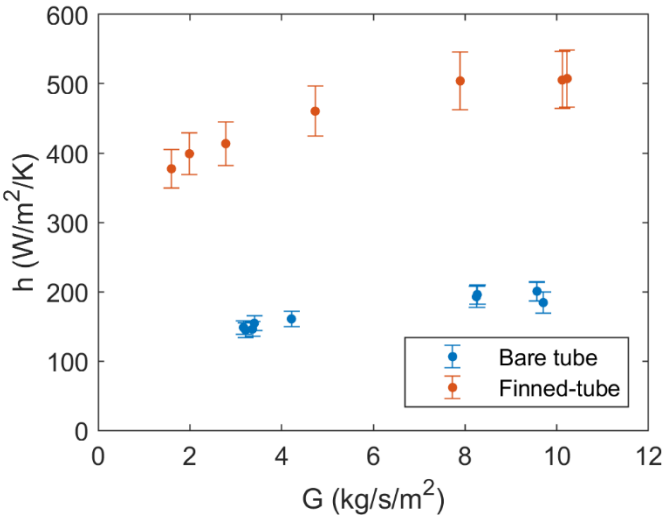

Figure 5: Measured convective HTC vs mass flux for bare-tubes compared to finned-tubes. Finned-tube HTC is calculated on the basis of bare-tube heat transfer area, which is approximately 18% of the total available geometric heat transfer area. Test ID: B1.1 vs F1.1

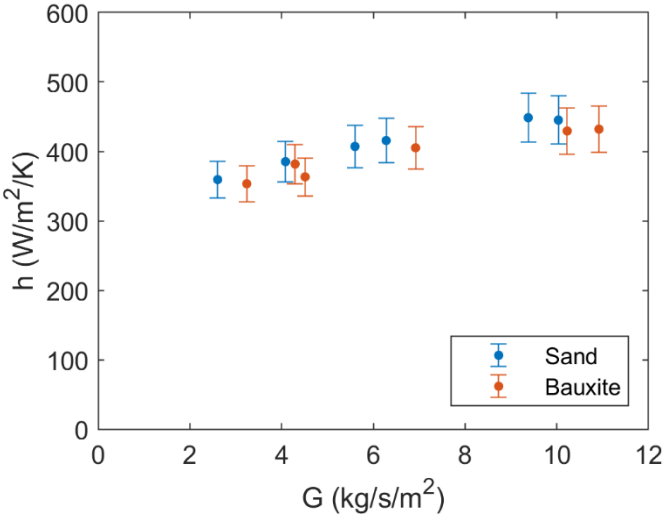

Figure 6: Measured convective HTC vs mass flux for finned tubes with quartz sand compared to sintered bauxite. Test ID: F1.2 vs F1.3

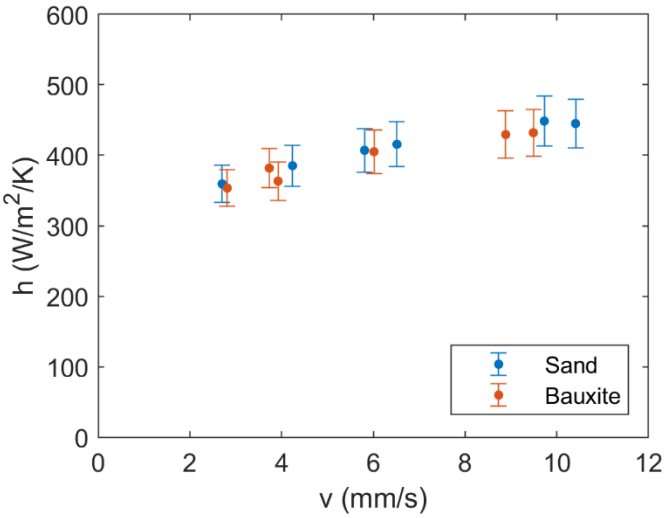

Figure 7: Measured convective HTC vs velocity for finned tubes with quartz sand compared to sintered bauxite. Here, the differing bulk densities of sand and bauxite are taken into account by calculating the particle velocity at the opening of the heat transfer section. When compared in this manner, the sand and bauxite data are said to be equivalent. Test ID: F1.2 vs F1.3

Figure 8 and Figure 9 show the effect of increasing horizontal tube spacing and tube diameter respectively. Increasing tube spacing decreases the measured HTC, while increasing tube diameter increases the HTC.

Figure 10 shows that increasing the fin pitch increases the measured HTC. Importantly, no ill-effects on HTC or particle flow were observed at the extreme fin pitch value of 394 fins/m, or 0.00216 m face-to-face spacing, which was the tightest spacing that could be sourced with the required fin height and thickness. This test used sintered bauxite with the relatively large mean particle diameter of 350 μm, such that the face-to-face spacing of the fins is only 6.2 times that of the particle diameter. Observation via the clear polycarbonate sheeting of the heat exchanger test section did not suggest any clogging or funnel flow developing at this extreme flow condition. This suggests that tight fin spacing can be used to maximize the heat transfer area to heat exchanger volume ratio without creating thick boundary layers of stagnant particles.

Figure 11 illustrates that measured HTC increases as fin height increases. The tested fin height range (6.4 mm – 12.7 mm) corresponds to the minimum and maximum fin heights that could be manufactured with the tested tube diameter of 19.1 mm.

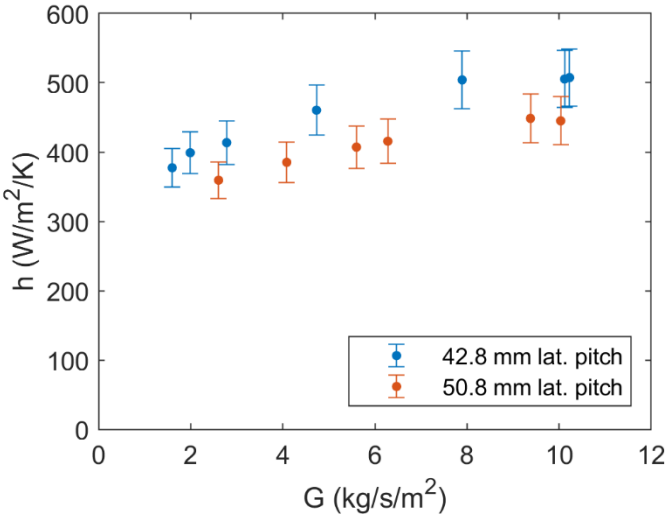

Figure 8: Measured convective HTC for two tube bundle orientations with differing horizontal pitch. Test ID: F1.1 vs F1.2

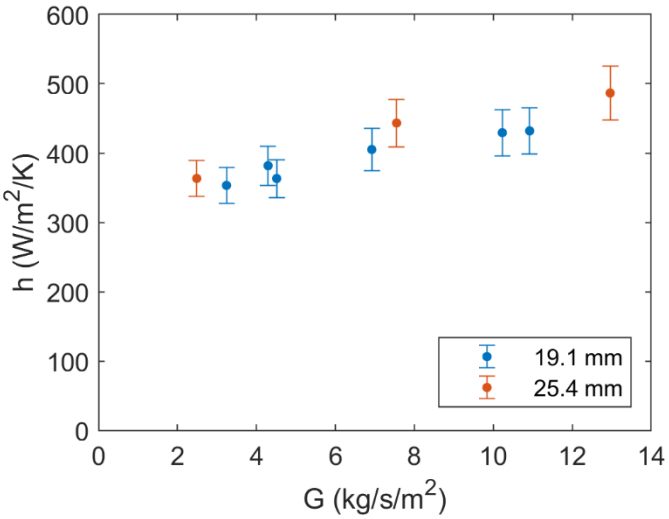

Figure 9: Measured convective HTC for differing tube diameters. Test ID: F1.3 vs F6.1

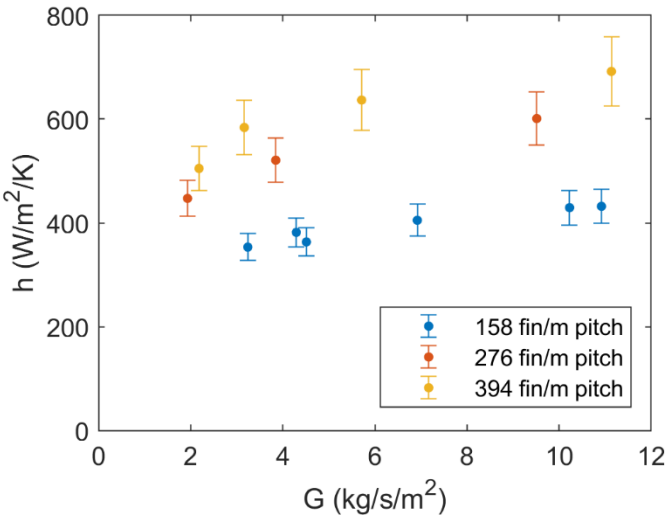

Figure 10: Measured convective HTC for differing fin pitch. Test ID: F1.3 vs F2.1 vs F4.1

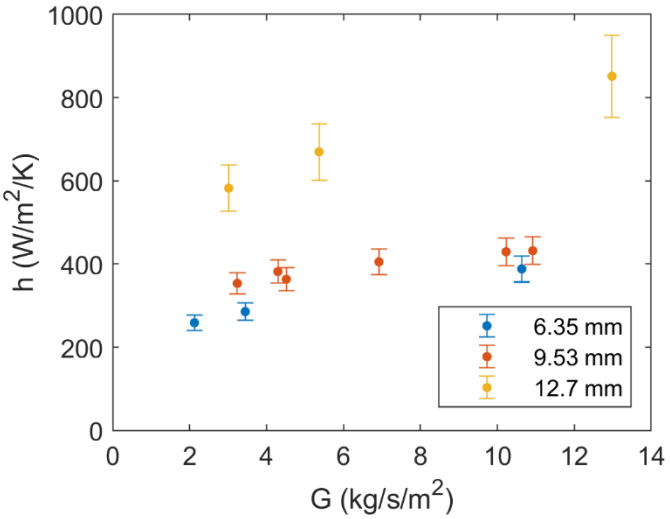

Figure 11: Measured convective HTC with differing fin height. Test ID: F3.2 vs F1.3 vs F5.1

The overall convective coefficient can be calculated as the inverse of the thermal resistance of the particle bed multiplied by the total heat transfer surface area of the tube.

$$h_{particle} = \left(R_{tot} A_{h,eff}\right)^{-1} \tag{3}$$

In this and the following equations, the effective heat transfer area includes the impact of fin efficiency on the fin area ($A_{h,eff} = A_{tube} + \eta_f A_{fin}$). The total thermal resistance of the convective process of the particle bed can be represented by the sum of the contact resistance and convective transport process within the particle bed:

$$R_{tot} = R_{contact} + R_{convective} \tag{4}$$

The contact resistance can be represented by:

$$R_{contact} = \frac{d_p}{2 k_{w,eff} A_{h,eff}} \tag{5}$$

where $k_{w,eff}$ is the effective near-wall thermal conduction coefficient (see equations 19-20 of [8] for details), and d_p is the mean particle diameter. The particle convective resistance is calculated by:

$$R_{convective} = \left(h_p A_{h,eff}\right)^{-1} \tag{6}$$

The convection coefficient is calculated from the Nusselt number based on the hydraulic diameter of a finned tube:

$$h_p = \frac{Nuk_{eff}(T)}{D_h} \tag{7}$$

$$D_h = \frac{\frac{d_f^2 - d_t^2}{2s_f} + \frac{d_f t_f}{s_f} + d_t\left(1 - \frac{t_f}{s_f}\right)}{1 + \frac{d_f - d_t}{s_f}} \tag{8}$$

The Nusselt number is assumed to follow a power-law trend with maximum particle velocity:

$$Nu = \alpha\left(\frac{v_{p,max}}{10\,mm/s}\right)^{\beta} \tag{9}$$

The maximum particle velocity is calculated by,

$$v_{p,max} = \frac{\dot{w}_{particle}}{\rho_{particle} A_{flow,min}} \tag{10}$$

where $A_{flow,min}$ is the minimum particle flow area based on calculated blockage, and accounts for tube spacing, diameter, etc. The effective thermal conductivity is assumed to follow a linear trend with temperature and is dependent on the particle media (Figure 12):

$$k_{eff} = A + B(T - 20°C) \tag{11}$$

The appropriate geometric parameters were calculated from each tubing configuration and substituted into the equations above. For each configuration, the parameters α and β were varied to minimize the root mean squared difference between the calculated HTCs and the measured values. The test conditions and calculated correlational parameters α and β are listed below in Table 2. A selection of test configuration data and the correlated HTC on a basis of bare tube area are shown in Figure 13. The same data and correlations are shown in Figure 14 on a basis of actual tube area.

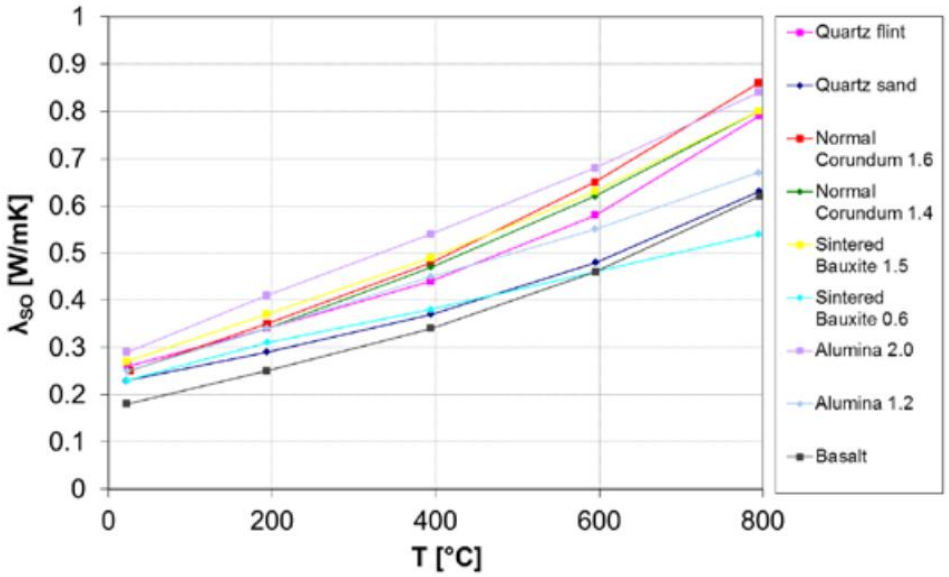

Figure 12: Packed bed thermal conductivity as a function of temperature for several materials. From [9].

ID	Config	Tube		Fin			Particle	Velocity (mm/s)	α	β
		Diameter (mm)	Lateral pitch (mm)	Height (mm)	Pitch (1/m)	Thickness (mm)				
B1.1	Bare	19.1	38.1	-	-	-	Sand	4-12	13.4	0.33
F1.1	Finned	19.1	42.9	9.5	158	0.4	Sand	2-12	14.8	0.26
F1.2	Finned	19.1	50.8	9.5	158	0.4	Sand	3-11	12.6	0.29
F1.3	Finned	19.1	50.8	9.5	158	0.4	Bauxite	3-10	12.1	0.30
B1.2	Bare	19.1	50.8	-	-	-	Bauxite	3-11	12.1	0.34
F2.1	Finned	19.1	50.8	9.5	276	0.4	Bauxite	2-9	11.3	0.32
F2.2	Finned	19.1	42.9	9.5	276	0.4	Bauxite	1-6	14.1	0.37
F3.1	Finned	19.1	42.9	6.4	158	0.4	Bauxite	2-7	13.8	0.42
F3.2	Finned	19.1	50.8	6.4	158	0.4	Bauxite	2-9	11.3	0.36
F4.1	Finned	19.1	50.8	9.4	394	0.4	Bauxite	2-10	8.4	0.22
F5.1	Finned	19.1	50.8	12.7	158	0.8	Bauxite	3-12	25.2	0.47
F6.1	Finned	25.4	50.8	9.5	158	0.4	Bauxite	2-12	15.5	0.29

Table 2: Reproduction of test configurations from Table 1 with correlation parameters α and β.

Conclusions

The correlational models developed in the present study are of particular interest in the development of a pilot scale particle-to-sCO_2 heat exchanger. As demonstrated by Baumann and Zunft [7] tubular MBHE designs yield similar convective HTC values as MB/PCHE. As demonstrated in the present study, the use of finned tubes to increase the ratio of heat transfer area to heat exchanger volume is expected to greatly increase the equivalent-area convective HTC compared to bare tube configurations. Importantly, no significant flow disruptions were observed during testing with finned tubes, suggesting MB/FTHE designs are a strong candidate for pilot scale testing with sCO_2. Within the bounds of the test parameters, no penalties to the measured convective HTC were found when increasing the density of the heat transfer material within the heat exchanger volume. Increasing tube diameter, fin height, and fin thickness and decreasing tube spacing and fin spacing are all shown to have positive effects on the convective HTC. The limit to these relationships was not found by the present study, however, the tested geometric parameters are within the typical design constraints for tubular heat exchangers and extreme deviations in full scale MB/FTHE design are not expected.

The trends in Figure 14 do suggest that diminishing returns are expected as heat transfer area is increased. The lowest true area heat transfer coefficient corresponds to the tube with the largest surface area. Economic analysis is required to find the breakeven point for a given construction in which adding additional heat transfer area adds more in construction cost than benefit in thermal efficiency.

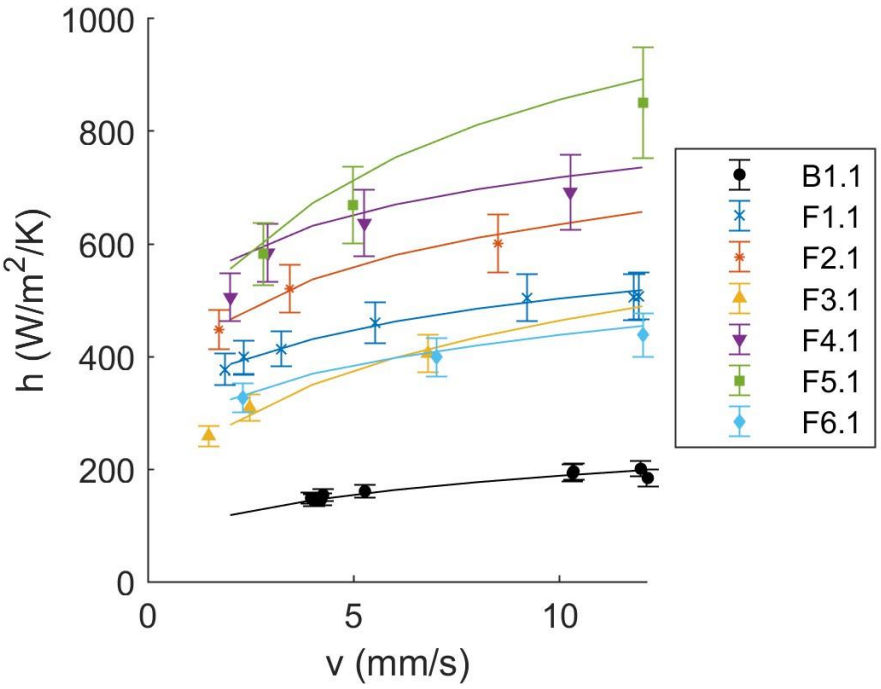

Figure 13: Modeled output (lines) correlated with measured convective HTC (points) for differing test configurations corresponding to test IDs from Table 2. For clarity not all test configurations are shown. Reported HTCs are calculated using the equivalent bare tube area to allow for direct comparison.

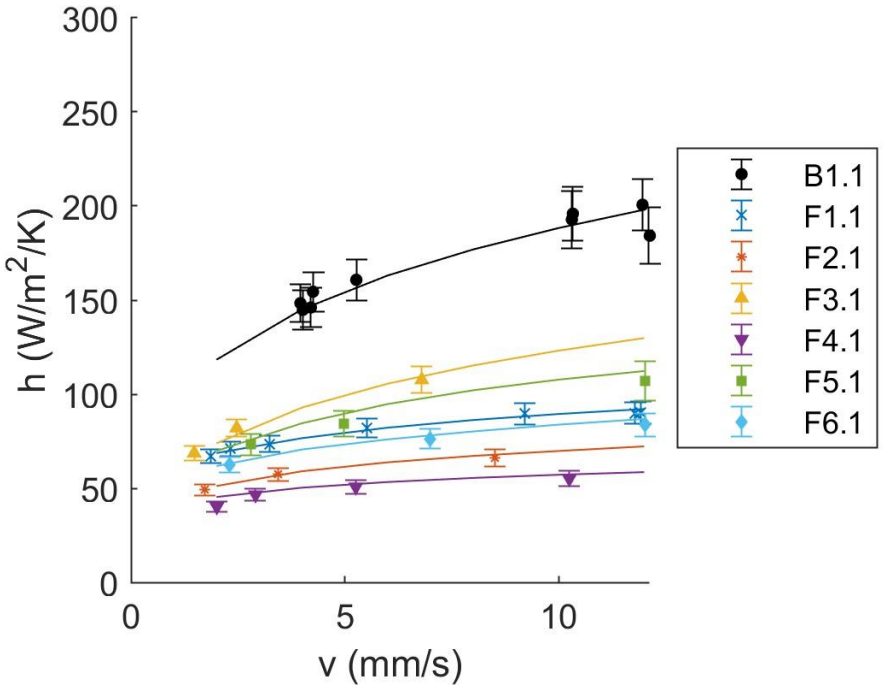

Figure 14: Modeled output (lines) correlated with measured convective HTC (points) for differing test configurations corresponding to test IDs from Table 2. For clarity not all test configurations are shown. Reported HTCs are calculated using the actual tube area.

Acknowledgement and Disclaimer

Thank you to Dr. Greg Mehos for providing consultation on the design of the test hopper to ensure proper flow conditions were maintained.

This material is based upon work supported by the U.S. Department of Energy, Office of Science, Office of Energy Efficiency and Renewable Energy, under Award Number(s) DE-SC0021717.

References

[1] K Schwaiger et al. “sandTES-A novel thermal energy storage system based on sand”. In: *21st International Conference on Fluidized Bed Combustion*, Naples, Italy. 2012.

[2] Ashley Dean Byman, Thomas Layne Charles, and Xingcun Huang. “Heat exchanger for cooling or heating bulk solids”. US2014/0246184A1. Sept. 2014.

[3] Ashley Dean Byman, Thomas Layne Charles, and Xingcun Huang. “Heat exchanger for cooling or heating bulk solids”. US2018/0347918A1. Dec. 2018.

[4] Ashley D. Byman et al. “Plattenwarmetauscher zur erwarmung oder kuhlung von schuttgut”. EP Patent Application EP18889479.4A. 2018

[5] Clifford K Ho. *High-temperature particle heat exchanger for sCO2 power cycles*. 2016. url: https://www.osti.gov/servlets/purl/1365201.

[6] Hendrik F. Laubscher, Kevin J. Albrecht, and Clifford K. Ho. “High-temperature particle flow testing in parallel plates for particle-to-supercritical CO2 heat exchanger applications”. In: *ASME 2020 14th International Conference on Energy Sustainability*. ASME Paper No. ES2020-1664. June 2020.

[7] T. Baumann and S. Zunft. “Development and performance assessment of a moving bed heat exchanger for solar central receiver power plants”. In: *Energy Procedia 69* (May 2015), pp. 748–757.

[8] Kevin J. Albrecht and Clifford K. Ho. “Heat transfer models of moving packed-bed particle-to-sCO2 heat exchangers”. In: *Journal of Solar Energy Engineering 141* (2017), p. 031006.

[9] T. Baumann and S. Zunft. “Properties of granular materials as heat transfer and storage medium in CSP application”. In: *Solar Energy Materials and Solar Cells 143* (Dec. 2015), pp. 38–47.

[10] Special Metals – A PCC Company. *INCONEL Alloy 740H*. 2015. url: https://www.specialmetals.com/assets/smc/documents/alloys/inconel/inconel-alloy-740-h.pdf.

[11] Greg Mehos. *Hopper design principles for chemical engineers.* Morris Publishing, Kearney, NE, 2018.

[12] Southall, D., 2009, “Diffusion Bonding in Compact Heat Exchangers,” *SCCO2 Power Cycle Symposium*, Troy, New York.

[13] Southall, D., and Dewson, S. J., 2010, “Innovative Compact Heat Exchangers,” *Proceedings of ICAPP ‘10*, San Diego, California, pp. 218--226.